applied sciences

MDPI

Article

Spectroscopic Characterization of Iron Slags from the Archaeological Sites of Brâncoveneşti, Călugăreni and Vătava Located on the Mureş County (Romania) Sector of the Roman *Limes*

Enikő Bitay [1,2,*], Irina Kacsó [3], Claudiu Tănăselia [4], Dana Toloman [3], Gheorghe Borodi [3], Szilamér-Péter Pánczél [5,6], Zsombor Kisfaludi-Bak [2] and Erzsébet Veress [2,*]

1 Faculty of Technical and Human Sciences, Sapientia Hungarian University of Transylvania, Op. 9, Cp. 4, 540485 Târgu-Mureş, Romania
2 Research Institute of the Transylvanian Museum Society, 2–4 Napoca, 400009 Cluj, Romania; kisfaludi.zsombor@eme.ro
3 National Institute for Research and Development of Isotopic and Molecular Technologies, 65–103 Donath, 400293 Cluj, Romania; irina.kacso@itim-cj.ro (I.K.); danag@itim-cj.ro (D.T.); borodi@itim-cj.ro (G.B.)
4 NCDO-INOE 2000 Research Institute for Analytical Instrumentation, 67 Donath, 400293 Cluj, Romania; claudiu@tanaselia.ro
5 Faculty of History, Babeş-Bolyai University, 1 Mihail Kogălniceanu, 400084 Cluj, Romania; pasz193518@studmail.ubbcluj.ro
6 Mureş County Museum, 8A Mărăşti, 540328 Târgu-Mureş, Romania
* Correspondence: bitay@eme.ro (E.B.); veresserzsebet@eme.ro (E.V.)

Received: 7 July 2020; Accepted: 31 July 2020; Published: 4 August 2020

Abstract: Iron slag samples unearthed from archaeological sites lying on the Eastern limes sector of Roman Dacia (the Brâncoveneşti and Călugăreni auxiliary forts and the Vătava watchtower) were studied in order to assess the probability of local iron working (smelting and smithing) during the 2nd–3rd centuries CE. Structural-mineralogic aspects revealed by PXRD analysis and FTIR spectroscopy indicate different slag types corresponding to different iron production and processing stages allowing the supposition that refining of the bloom and processing of the refined iron took place on the sites. The FTIR absorption bands obtained in the spectral domain 2000–400 cm^{-1} show that mineralogically the samples are constituted mainly of silicates associated with minor quantities of aluminates and carbonates. The fayalite, haematite, and magnetite phases appearing on both the X-ray diffractograms and the FTIR spectra agree with the redox conditions of the slag formation process which result from the Fe^{3+}/Fe^{2+} ratio determined using the EPR-method. The bulk macro-elemental PXRF and ICP-MS spectroscopy data support the slag typization proposed on the basis of the probable working conditions; trace-elemental bulk composition suggests that the provenance of the raw materials may be different.

Keywords: iron slags; roman; field portable X-ray fluorescence spectroscopy; inductively coupled plasma mass spectrometry; Fourier transform infrared spectroscopy; powder X-ray diffraction; electron paramagnetic resonance spectroscopy

1. Introduction

The iron slag samples investigated in the present study were unearthed at three major archaeologic sites located on the Eastern frontier (*limes*) of Roman Dacia, in today Mureş County, Romania (Figure 1). At Brâncoveneşti (Hungarian name: Marosvécs) and Călugăreni (Mikháza), the remains of the Roman auxiliary forts and the adjacent military settlements are known since the 18th and 19th century.

The fortlet (watchtower) identified at Vătava (Felsőrépa) during a field survey in 2011 is supposed to be closely linked to the Brâncoveneşti fort. Relying on the natural protection offered by the nearby mountains and hills, the defensive structures of the eastern *limes* controlled the main traffic routes towards the *barbaricum*. The Brâncoveneşti fort, assisted by watchtowers, monitored the border section towards the upper Mureş Valley (Felső Maros-mente), whilst the Călugăreni fort supervised the upper Niraj Valley (Felső Nyárád-mente). In the 2nd and 3rd centuries centuries AD, both forts were strategically important military locations of the eastern border of the Dacian provinces.

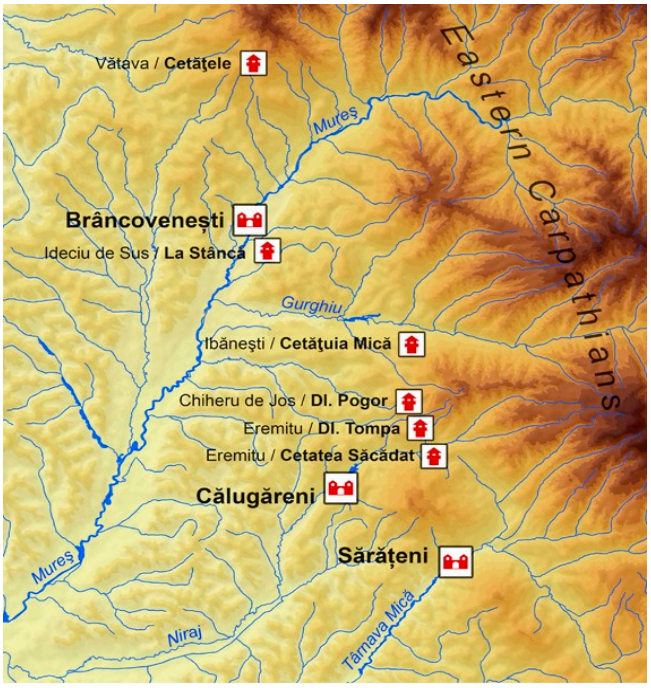

Figure 1. Roman fortifications on the eastern Dacian limes on today Mureş County (© Szabó Máté).

During the research excavations carried out at Brâncoveneşti and Călugăreni, in the military forts and the adjacent settlements (*vici*) as well as at the watchtower from Vătava, plenty of Roman material was recovered, mainly ceramic vessels, building materials and animal bones, but also stone, bone, glass, iron and copper alloy artifacts. At each location, rich iron slag deposits have been found; at Vătava, even some blacksmithing tools have been recovered [1–4]. The multitude of the iron slags indicate the presence of some kind of metallurgical workshops; however, up to now, neither smelter (furnace) nor smithery remains weren't discovered, so presently the exact whereabouts of the presumably practiced activity is unknown.

Knowledge on the slag finds' chemical-mineralogical composition and their microstructural analyses could enable to identify the remains as smelting byproducts or primary/secondary smithing debris. The value of the Fe^{3+}/Fe^{2+} ratio, defined mainly by the redox condition evolved during each particular stage of processing, could allow us to conclude if iron-producing or iron-working took place at either location.

The present study is focused primarily on the elemental analysis of the slag samples. Chemical composition was determined by PXRF (Field Portable X-ray Fluorescence Spectroscopy) and ICP-MS (Inductively Coupled Plasma Mass Spectrometry). In addition, structural-mineralogical investigation of selected samples was carried out by PXRD (Powder X-ray Diffraction) and FTIR (Fourier Transform Infrared) spectroscopy, and the Fe^{3+}/Fe^{2+} ratio was determined using EPR (Electron Paramagnetic Resonance) spectroscopy measurements. The information acquired facilitate the categorization of the finds and could shed some light on the nature of the metallurgical activity practiced

at the archaeological sites in question (iron production, refining or processing), the metallurgical techniques used, and on the closer provenance or more distant sourcing of the raw materials used [5–7].

2. Materials and Methods

The study continues the preliminary characterization started on 17 iron slag smallfinds deriving from Călugăreni [8]. The samples investigated in the present phase (Table 1) came from the Călugăreni auxiliary fort *principia* (headquarter building), from the Călugăreni *vicus*, the civil settlement evolved next to the fort, from the *retentura* ("backyard") of the principia of the Brâncoveneşti auxiliary fort, and one representative find from Vătava, East of the tower location.

Table 1. The iron slag samples.

Site Location	Smallfind No.	Trench	Context	Fieldwork Year
Brâncoveneşti, *retentura*	9487	A	1	2012
	9454	A	3	2012
	9445	A	3	2012
Călugăreni, *vicus*	2008	C	2000	2013
	2155	C	2001	2013
	2318	C	2005	2013
	2342	C	2005	2013
	2355	C	2009	2013
	2356	C	2009	2013
	4009	C2	2039	2014
	4137	C1	2034	2014
	4169	C2	2039	2014
	4222	C1	2038	2014
	4251	C1	2035	2014
	4264	C1	2038	2014
Călugăreni, *principia*	10218	A2	109	2015
	10532	A5	250	2016
	10661	A5	339	2016
	10673	A	346	2016
	11145	A6	443	2017
Vătava, *East of the tower*	Vat	V		2014

Surface macro- and micro-elemental composition of the samples was characterized by PXRF measurements carried out in three different points of the carefully cleaned finds, using an INNOV-X Alpha-6500 spectrometer (Olympus, Woburn, MA USA) (spot size 2 mm^2, 35 kV, 15 μA, 3 mm filter, Be window, PIN Si detector, counting time 60 s in two consecutive 30 s runs).

Bulk macro- and micro-elemental compositions were determined, in parallel, by PXRF and ICP-MS measurements.

For the bulk PXRF measurements, the same PXRF spectrometer was used, the analysis being performed on three disc-shaped pellets (d = 1 cm) prepared from each sample by pressing 1.00 ± 0.05 g amounts of the finely pulverized (<63 μm) material grinded in agate mill, after the external (environmentally contaminated and possibly weathered) layer removed.

Despite the typical bias of the acquired data as compared to the results of the usual wet laboratory measurements, PXRF is presently a routine field analytical method for elements with medium to high atomic mass (K to U), in the concentration range of a few mg/kg to a few %. The differences can be attributed to the basically different sample preparation and measurement methodology (point-and-shoot surface measurement vs. bulk measurement on homogenized samples), chemical matrix effects (particularly at high Fe contents), matrix heterogeneity, and spectral interferences. Detection limits vary with sample matrix composition; high abundance of heavier major elements, mainly iron, negatively affects trace element detection [9]. PXRF spectrometry can't accurately quantify

lighter elements (e.g., Na, P), nor Ti, V, Cr, Co, Ni and Ba at their typical concentrations in slag-like matrices, and its reliability is unsatisfactory in the case of the trace elements [10]. Consequently, PXRF generally can reliably provide qualitative (at best semiquantitative) data; gathering of quantitative data is problematic, particularly when the material is heterogeneous in nature. In case of iron slag samples analyzed in parallel with the PXRF method and wet chemistry, the PXRF analytical performance is defined by its <30% error, in samples containing very low or very high quantities of the analyzed element the error reaching >30% [6].

In the present study, the samples of bulk elemental composition determined by PXRF was compared with the data obtained on the same probe by ICP-MS, chosen as the wet chemical analysis method. ICP-MS measurements were performed using an Elan DRC II quadrupole spectrometer (plasma power 1250 W; concentric nebulizer Meinhardt; argon flow 0.86 mL min^{-1}), on three 0.25 ± 0.05 g amounts of the same powdered bulk sample, solubilized following the total acid digestion method earlier presented [11]. For data processing, the TotalQuant semi-quantitative measurement mode of the Elan 3.4 software was used, with multiple point calibration for low, medium, and high masses. The method is less accurate for Na, Mg, Al, Si, K, and Fe; however, the accuracy is generally better than 15%, the detection limit being in the ppt (ng L^{-1}) range, without significant matrix effects above 1 ppm (1 µg L^{-1}) [12]. In this specific case, according to the value given by the instrument, the detection limit, LOD, was 0.02 mg kg^{-1} overall.

In order to characterize the slags from a mineralogical-structural point of view, FTIR spectroscopy and PXRD analysis were carried out on the pulverized bulk samples presented above; the FTIR spectra were recorded on the samples carefully removed, and also finely powdered external layer.

FTIR determinations were realized using a JASCO 6100 FTIR spectrometer (Manufacturer: JASCO Applied Sciences, Silver Spring, MD USA) (spectral domain: 4000 ¬ 400 cm^{-1}, resolution: 2 cm^{-1}, KBr pellet technique).

PXRD analysis was performed with a Bruker D8 Advance diffractometer (Bruker Corporation, Billerica, MA, USA) working in Bragg-Brentano mode (acquisition conditions: $\lambda_{CuK\alpha1}$ = 1.5406 A, 40 kV, 40 mA, scan interval 5 to 70 degrees 2θ, step size 0.02 degrees 2θ, count time 2 s); observed peak positions were matched using the ICDD-JCPDS database.

The Fe^{3+}/Fe^{2+} ratio was determined by EPR spectroscopy at room temperature, using a Bruker ELEXSYS E500 X-band spectrometer (9.46 GHz) following the procedure previously presented [13]. EPR experiments were performed on 20 mg amounts of the finely powdered samples, firstly in absence of thermal conditioning, then after the quantitative oxidation of the total Fe^{2+} content by 6 h heating at 300 °C in atmospheric conditions. Data acquisition and processing were assured by the Bruker Xepr suite for ELEXSYS spectrometers.

3. Results and Discussion

3.1. Elemental Analysis

Archaeological iron slag is a complex, heterogeneous material with the major constitutive elements Al, Si, K, Ca, Ti, Mn, Fe, Sr, Zr, and Ba. The presence and the concentration level of Al, Si, Ca, Mn, Sr, and Ba are related to the choice of fluxes; K and Ca level is able to indicate the fuel sources used, while Fe, Ti, and Zr levels are indicative of the iron ore source [6].

Surface elemental composition data of the slags are presented in Table 2 (major elements) and Table 3 (trace elements); the measurements were carried out in three different superficial points of the carefully cleaned finds.

The mean surface elemental concentration values offer a good view on the samples' mineral-chemical heterogeneity.

The major elemental composition (Table 2) is dominated by Fe. Ca level is rather low, otherwise the slags are also poor in other major lithophile elements (notice that Na, Si, and Al could not be determined). Ti (2500–5500 ppm) was detected in samples 4264, 4009, 4169, 4222 (Călugăreni-*vicus*, Cal-v), 9487,

9454 (Brâncoveneşti-*retentura*, Br-r) and Vat (Vătava, *East of the* tower), while Ba (500–1500 ppm) in 4251, 4264, 4169, 4222 (Cal-v), 9487, 9445, and 9454 (Br-*r*). Mn (500–5500 ppm) and Sr (120–250 ppm) are overall present.

Table 2. PXRF surface analysis–major lithophile elements (mg kg^{-1}).

Element		Iron Slag Samples									
		4137	**4251**	**4264**	**4009**	**4169**	**4222**	**9487**	**9445**	**9454**	**Vat**
		C1/2034	**C1/2035**	**C1/2038**	**C2/2039**	**C2/2039**	**C1/2038**	**A/1**	**A/3**	**A/3**	**V**
Ca	LOD	1380	1300	770	1995	1024	949	1054	2607	1464	637
	Mean	21,297	33,228	38,532	24,263	44,573	17,696	20,754	49,613	30,540	3730
	Min	4107	24,077	30398	13,885	31,686	9693	11,256	36,136	24,470	3314
	Max	53,444	43,160	78,283	29,904	52,852	24,236	33,382	62,790	36,910	4146
	SD	27,862	9565	36,372	8999	11,310	7381	11,390	13,330	6230	588
	CV	1.308	0.288	0.944	0.371	0.254	0.417	0.549	0.269	0.204	0.158
Ti	LOD	2011	1848	300	521	1958	1784	1643	1585	1801	1975
	Mean			5765	2399	2300	5070	3494		2309	3255
	Min			5321	1677	2292	4591	2547		1870	2692
	Max	<LOD	<LOD	6356	3121	2307	5609	4441	<LOD	2938	3684
	SD			533	1021	11	512	1643		1801	1975
	CV			0.092	0.426	0.005	0.101	0.470		0.780	0.607
Mn	LOD	150	232	51	146	140	114	95	84	108	110
	Mean	1199	5330	1245	1790	3700	1177	1563	640	1143	1360
	Min	855	1814	707	1553	1484	978	1284	554	980	1190
	Max	1822	7534	1823	2152	4968	1486	2120	793	1261	1464
	SD	541	3078	559	319	1926	271	483	133	146	148
	CV	0.451	0.577	0.449	0.178	0.521	0.230	0.309	0.208	0.128	0.109
Fe	LOD	13,278	12,882	1394	7608	15,265	11,285	9749	9593	11,140	15,686
	Mean	338,675	279,243	66,312	277,967	275,126	174,988	276,220	342,819	250,103	398,613
	Min	288,777	267,913	44,686	177,197	243,677	119,587	193,649	322,470	242,344	363,707
	Max	376,258	298,660	107,359	400,462	337,235	274,060	357,994	371,565	259,135	418,451
	SD	45,022	16,893	35,557	113,207	53,790	85,999	82,175	25,602	8468	30,323
	CV	0.133	0.060	0.536	0.407	0.196	0.491	0.297	0.075	0.034	0.076
Sr	LOD	10	9	7	10	8	8	8	23	13	8
	Mean	124	180	156	160	212	242	135	277	224	24
	Min	44	133	133	107	163	86	95	122	173	22
	Max	282	231	283	188	336	349	157	481	327	25
	SD	137	49	78	46	109	138	35	185	89	2
	CV	1.105	0.272	0.500	0.288	0.514	0.570	0.259	0.668	0.325	0.083
Ba	LOD	175	164	60	122	174	155	141	142	158	491
	Mean		1529	432		1423	775	722	654	912	
	Min		1445	348		998	735	530	641	667	
	Max	<LOD	1639	594	<LOD	1699	814	1021	677	1111	
	SD		99	140		373	56	262	20	226	
	CV		0.065	0.324		0.262	0.072	0.363	0.031	0.248	

LOD: limit of detection; Mean: mean value of the measurements in three different surface points; SD: standard deviation; CV: coefficient of variation.

The slag surfaces are very poor in volatiles; however, in some samples, detectable amounts of As (4169) and Br (4137, 4251, 9445, 9454, Vat) were found.

The surfaces are relatively poor in trace elements too (Table 3). Co (at relatively high level) and Rb are present in all samples; in some cases, Zn (4251, 4264, 4169, 4222, 9487, 9454), Mo, and Pb (4137, 4251, 4009, 4169, 4222, 9487, 9445, 9454, Vat), respectively Bi (4137, 4251, 4009, 4169, 9445, 9454, Vat) were detected in significant amounts. Cu appears in measurable amount in two samples only (4169, 4222). The somewhat surprising presence of gold on the surface of samples 4137, 9454, and Vat was confirmed microscopically [8] (Au globules embedded by "accidental" contamination?). It should be noted that Au doesn't appear in the PXRF or the ICP-MS bulk results.

Table 3. PXRF surface analysis–trace elements (mg kg^{-1}).

Element		Iron Slag Samples									
		4137	**4251**	**4264**	**4009**	**4169**	**4222**	**9487**	**9445**	**9454**	**Vat**
		C1/2034	**C1/2035**	**C1/2038**	**C2/2039**	**C2/2039**	**C1/2038**	**A/1**	**A/3**	**A/3**	**V**
Co	LOD	105	108	17	66	148	105	93	90	108	217
	Mean	1117	589	92	583	1133	709	910	1515	848	2149
	Min	972	285	53	424	982	405	463	1237	666	2025
	Max	1359	949	169	858	1081	1117	1220	1912	1144	2285
	SD	211	355	67	239	183	367	397	353	259	130
	CV	0.189	0.603	0.728	0.410	0.162	0.518	0.436	0.233	0.305	0.060
Cu	LOD	101	100	14	78	127	107	26	48	22	76
	Mean					243	98				
	Min					239	76				
	Max	<LOD	<LOD	<LOD	<LOD	246	119	<LOD	<LOD	<LOD	<LOD
	SD					5	30				
	CV					0.021	0.306				
Zn	LOD	24	30	10	17	66	62	50	42	71	75
	Mean		764	68		131	164	94		130	
	Min		386	48		114	148	50		88	
	Max	<LOD	1118	88	<LOD	147	179	137	<LOD	172	<LOD
	SD		367	20		23	22	62		59	
	CV		0.480	0.294		0.176	0.134	0.660		0.454	
As	LOD	42	44	14	27	57	43	40	36	21	77
	Mean					28					
	Min					27					
	Max	<LOD	<LOD	<LOD	<LOD	29	<LOD	<LOD	<LOD	<LOD	<LOD
	SD					1					
	CV					0.036					
Br	LOD	7	6	4	6	8	6	8	7	9	11
	Mean	39	29						35	29	46
	Min	29	20						26	27	43
	Max	46	36	<LOD	<LOD	<LOD	<LOD	<LOD	50	31	51
	SD	9	8						13	3	4
	CV	0.231	0.276						0.371	0.103	0.087
Rb	LOD	8	7	5	5	10	8	7	16	8	13
	Mean	60	52	73	57	49	88	70	65	50	86
	Min	50	49	62	38	39	78	44	53	33	80
	Max	68	56	91	70	55	94	108	71	75	91
	SD	9	4	16	17	9	9	34	11	22	6
	CV	0.150	0.077	0.219	0.298	0.184	0.102	0.486	0.169	0.440	0.070
Zr	LOD	8	8	7	8	7	8	8	7	10	10
	Mean	57	97	185	122	81	137	122	33	126	100
	Min	41	91	151	82	60	121	85	26	118	87
	Max	72	101	214	142	96	147	192	40	134	115
	SD	16	5	32	34	19	14	61	7	8	14
	CV	0.281	0.052	0.173	0.279	0.235	0.102	0.500	0.212	0.063	0.140
Mo	LOD	23	22	41	20	25	22	20	20	24	35
	Mean	211	114		88	139	108	136	194	114	293
	Min	134	76		60	121	84	85	178	99	253
	Max	199	163	<LOD	118	153	131	156	221	140	337
	SD	84	44		29	17	33	71	24	23	42
	CV	0.398	0.386		0.330	0.122	0.306	0.522	0.124	0.202	0.143
Au	LOD	31	32	16	22	34	25	30	28	38	46
	Mean	46							43		66
	Min	44							36		59
	Max	47	<LOD	<LOD	<LOD	<LOD	<LOD	<LOD	49	<LOD	73
	SD	2							9		10
	CV	0.043							0.209		0.152

Table 3. *Cont.*

Element		Iron Slag Samples									
		4137	**4251**	**4264**	**4009**	**4169**	**4222**	**9487**	**9445**	**9454**	**Vat**
		C1/2034	**C1/2035**	**C1/2038**	**C2/2039**	**C2/2039**	**C1/2038**	**A/1**	**A/3**	**A/3**	**V**
Pb	LOD	25	28	21	15	39	26	22	19	26	53
	Mean	442	316		104	281	96	921	406	157	527
	Min	359	122		56	160	67	75	214	105	485
	Max	534	673	<LOD	164	393	119	2107	510	208	610
	SD	88	309		55	117	26	1058	167	52	72
	CV	0.199	0.978		0.529	0.416	0.271	1.149	0.411	0.331	0.137
Bi	LOD	10	11	12	19	15	10	9	8	10	22
	Mean	119	33		40	49			120	38	176
	Min	52	29		34	36			75	27	163
	Max	155	42	<LOD	46	61	<LOD	<LOD	145	52	199
	SD	58	12		8	18			39	13	20
	CV	0.487	0.364		0.200	0.367			0.325	0.342	0.114

LOD: limit of detection; Mean: mean value of the measurements in three different surface points; SD: standard deviation; CV: coefficient of variation.

PXRF bulk data (Table 4) generally agree with the similarly determined surface data; however, there are some differences.

The dominant lithophile element of the bulk is Fe. Ca level is relatively low, the slags being generally poor in lithophiles excepting Fe. On the surface, K is not detected, and even in the bulk appears in sample 4264 only (9500 mg kg^{-1}). Contrary to the surface data where Ti is present in almost all samples, in the bulk samples, PXRF is detected in 4264 and 4009 alone (3500–4500 mg kg^{-1}). Ba is present in all Brâncoveneşti and Călugăreni samples, missing that from Vătava (Vat).

Concerning the trace elements, Cu is present in sample 4264 only; Zn in 4137, 4251, 4264, 4009; and As in 9454. Rb is missing from 9445, Mo from 4264, Pb from 4264, and Bi from 4264 and 4009. Sn appears in samples 4251, 9487, and 9445. Br, originating probably from the local wood fuel used [14,15], is overall present.

ICP-MS data of the samples' bulk elemental composition are presented in Table 5 (according to the value given by the measuring instrument, LOD is overall 0.02 mg kg^{-1}).

PXRF and ICP-MS bulk data differ significantly, as both the required sample preparation methodology and the concentration ranges characterizing the analytical methods are different (for example, measuring the same samples by using the more sensitive ICP-MS method, the presence and concentration level of further trace elements—Cr, Ni, Ag, Cd, Sb, I—could be determined, whilst Ca and Br couldn't be measured). Commonly, it can be stated that, at concentration levels of 50–100 mg kg^{-1} or more, PXRF data should be considered more reliable, while, below 50 mg kg^{-1}, the ICP-MS values are more creditable [16,17].

However, the general trend of the elemental concentrations measured by PXRF and ICP-MS is running parallel, especially when speaking on the slags' major elements.

Bulk and surface chemical compositions equally suggest that at least bloom refining and/or the refined iron processing took place on the sites investigated. The slag samples seem to be most of all byproducts of the bloom refining process carried out in pit-furnaces.

Concluding about questions related to the provenance of raw materials (including the raw bloom supposed to be refined) would be very difficult as the quantity of the slag pieces collected was individually far below the recommended minimal amount of 200–300 g recommended for reliable bulk analysis of such highly heterogeneous materials [18–20].

Table 4. PXRF bulk analysis—major and trace elements (mg kg^{-1}).

Element	Iron Slag Samples									
	4137	**4251**	**4264**	**4009**	**4169**	**4222**	**9487**	**9445**	**9454**	**Vat**
	C1/2034	**C1/2035**	**C1/2038**	**C2/2039**	**C2/2039**	**C1/2038**	**A/1**	**A/3**	**A/3**	**V**
Major (lithophile) elements										
K	<LOD	<LOD	9468 ± 1278	<LOD	<LOD	<LOD	<LOD	<LOD	<LOD	<LOD
Ca	22,013 ± 1380	20,730 ± 1300	21,251 ± 770	44,499 ± 1995	12,968 ± 1024	13,638 ± 949	17,736 ± 1054	56,950 ± 2607	26,035 ± 1464	3582 ± 637
Ti	<LOD	<LOD	4432 ± 300	3298 ± 521	<LOD	<LOD	<LOD	<LOD	<LOD	<LOD
Mn	2096 ± 150	4285 ± 232	1148 ± 51	2868 ± 146	1597 ± 140	1342 ± 114	974 ± 95	549 ± 84	1140 ± 108	546 ± 110
Fe	299,949 ± 13,278	296,537 ± 12,882	52,900 ± 1394	202,134 ± 7608	336,825 ± 15,265	272,201 ± 11,285	246,979 ± 9749	241,312 ± 9593	265,946 ± 11,140	344,567 ± 15,686
Sr	162 ± 10	131 ± 9	185 ± 7	197 ± 10	78 ± 8	110 ± 8	111 ± 8	607 ± 23	231 ± 13	35 ± 8
Ba	982 ± 175	802 ± 164	315 ± 60	504 ± 122	721 ± 174	838 ± 155	782 ± 141	898 ± 142	932 ± 158	<LOD
Trace elements										
Co	815 ± 105	730 ± 1088	102 ± 17	343 ± 66	1533 ± 148	1002 ± 105	898 ± 93	826 ± 90	530 ± 108	1138 ± 217
Cu	<LOD	<LOD	55 ± 14	<LOD	<LOD	<LOD	<LOD	<LOD	<LOD	<LOD
Zn	102 ± 24	227 ± 30	80 ± 10	70 ± 17	<LOD	<LOD	<LOD	<LOD	<LOD	<LOD
As	<LOD	<LOD	<LOD	<LOD	<LOD	<LOD	<LOD	< LOD	150 ± 21	<LOD
Br	29 ± 7	34 ± 6	34 ± 4	28 ± 6	41 ± 8	24 ± 6	56 ± 8	22 ± 7	36 ± 9	61 ± 11
Rb	54 ± 8	33 ± 7	97 ± 5	32 ± 5	72 ± 10	62 ± 8	54 ± 7	<LOD	50 ± 8	74 ± 13
Zr	79 ± 8	73 ± 8	193 ± 7	119 ± 8	53 ± 7	80 ± 8	103 ± 8	27 ± 7	136 ± 10	76 ± 10
Mo	154 ± 23	153 ± 22	<LOD	77 ± 20	210 ± 25	145 ± 22	106 ± 20	100 ± 20	171 ± 24	295 ± 35
Sn	<LOD	219 ± 73	<LOD	<LOD	<LOD	<LOD	254 ± 67	193 ± 63	<LOD	<LOD
Pb	154 ± 25	230 ± 28	<LOD	45 ± 15	402 ± 39	219 ± 26	154 ± 22	70 ± 19	156 ± 26	383 ± 53
Bi	46 ± 10	74 ± 11	<LOD	<LOD	132 ± 15	53 ± 10	56 ± 9	42 ± 8	43 ± 10	146 ± 22

Uncertainty values are instrument-calculated for each element in each matrix; LOD: limit of detection.

Table 5. The slags elemental composition, ICP-MS analysis data (mg kg^{-1}).

Element	Iron Slag Samples									
	4137	**4251**	**4264**	**4009**	**4169**	**4222**	**9487**	**9445**	**9454**	**Vat**
	C1/2034	**C1/2035**	**C1/2038**	**C2/2039**	**C2/2039**	**C1/2038**	**A/1**	**A/3**	**A/3**	**V**
Major elements										
K	1408.08	913.50	1982.75	984.88	209.88	627.52	720.45	264.74	585.83	296.72
Ca	Not determined									
Ti	280.14	294.44	553.48	509.61	50.57	133.33	149.85	76.75	156.53	64.67
Mn	487.34	1401.13	138.83	824.49	186.59	141.40	107.52	55.13	147.38	37.25
Fe	98,280.59	51,784.61	6301.41	23,665.16	39,406.19	29,227.91	26,011.80	30,914.23	39,863.00	43,669.51
Sr	21.61	14.11	49.57	47.45	12.81	14.14	13.38	97.02	77.57	6.59
Ba	1293.97	211.53	56.97	103.57	125.12	417.10	130.90	594.43	601.68	48.35
Trace elements										
Cr	12.93	6.73	10.73	9.29	1.82	3.93	3.05	2.24	8.17	1.20
Co	4.42	1.18	0.86	0.82	8.15	2.98	2.69	2.47	0.91	4.42
Ni	15.37	8.56	7.60	9.31	3.02	3.42	3.01	59.52	13.72	1.01
Cu	17.55	7.51	49.15	12.15	6.55	5.00	6.04	7.00	5.92	2.56
Zn	22.51	25.13	13.06	11.99	2.27	2.12	2.55	6.39	9.41	0.10
As	28.98	16.72	8.91	32.45	7.72	13.41	14.62	60.19	41.41	6.35
Br	Not determined									
Rb	4.07	2.33	11.33	1.97	9.70	6.64	3.72	1.47	3.64	8.72
Zr	0.97	0.65	11.84	2.45	0.46	1.39	1.74	0.34	8.12	0.50
Mo	1.63	1.80	0.14	1.31	4.56	3.08	0.98	0.81	3.71	5.60
Ag	0.32	0.20	0.11	0.19	0.06	0.05	0.03	0.07	0.20	<0.02
Cd	0.12	0.08	0.01	0.05	0.05	0.04	0.02	0.04	0.05	<0.02
Sn	0.16	0.77	0.32	0.21	0.11	0.12	0.86	0.52	0.33	0.20
Sb	0.25	0.18	0.02	0.13	0.56	0.17	0.13	0.05	0.07	0.03
I	0.03	<0.02	0.02	0.03	<0.02	<0.02	<0.02	<0.02	<0.02	<0.02
Pb	2.18	2.72	0.17	0.81	10.33	2.29	1.98	0.67	1.99	4.81
Bi	<0.02	0.24	0.18	0.56	1.12	0.10	<0.02	0.15	0.05	1.68

3.2. PXRD Analysis

Ancient iron slags are mainly constituted of iron-bearing silicate minerals: olivine, typically fayalite (Fe_2SiO_4), pyroxene, frequently hedenbergite ($CaFe^{2+}Si_2O_6$), and glass, with iron oxide-hydroxide minerals—mostly wüstite (FeO), magnetite (Fe_3O_4), goethite (α-FeO(OH)), and metallic iron as minor common components. Short range mineralogical variations seen in slags suggest that, during formation, there were relative unstable oxygen and temperature conditions [21].

According to their mineral composition, iron slags can be divided into two main classes [22].

The first type is principally constituted of the typical iron oxide-hydroxide minerals: wüstite, magnetite, and the weathering products goethite and lepidocrocite (γ-FeO(OH)); then, an appreciable amount of quartz (SiO_2), glassy phases, and metallic iron. Wüstite is very common in bloomery slag; in smithing slag; where, during the slag formation, the temperature and/or oxygen content are high, instead of wüstite, magnetite occurs instead. Glass forms from the 'residual melt' and may vary considerably, depending on which minerals had previously crystallized, the total composition of the slag, and the progress of cooling. Droplets of few micrometers sized metallic iron formed during the reduction process are also common slag inclusions.

The major mineral phases of the more common second type are pyroxenes (hedenbergite), olivines (fayalite), and iron oxides, although olivine minerals and wüstite could be present only in small quantities or absent. The presence of (usually smaller quantities) of other minerals formed by firing at over 900 °C—mullite ($Al_6Si_2O_{13}$), cristobalite (SiO_2), pyrolusite (MnO_2), akermanite ($Ca_2Mg(Si_2O_7)$), etc.—can be ascribed on the account of furnace or smith's hearth linings; the silica polymorph cristobalite formed actually suggests a heating temperature of at least 1200 °C.

In case of the iron slag samples being selected for PXRD investigation, only part of the mineral components visible by petrographic microscopy [8] could be confirmed. While on the diffractograms recorded (Figure 2) some of the anterior detected minerals (quartz, cristobalite, goethite, magnetite, pyroxene) can be reliably identified, confirmation of the presence (and evaluation of the quantity) of other phases is difficult. Most of the finely disseminated, microscopically visible silicates crystallized in the glassy matrix (the fayalite and the coexisting hedenbergite) and part of the iron oxides (magnetite, haematite, wustite) could not be reliably evidenced due to the complex superposition of the minerals' individual PXRD pattern and to the signal degradation caused by the firing caused vitrification in addition to the amorphization occurring due to the burial environmental circumstances [23–25].

The semiquantitatively estimated most important components of the PXRD-analyzed samples are presented in Table 6.

Except for the Vat (Vătava) sample (very poor in quartz), the dominant crystalline phase is quartz, followed by cristobalite (though in some samples only in traces) and the (most probably weathering product) goethite. A large quantity of amorphous and/or glassy material was also evidenced. Magnetite and hedenbergite were detected in traces in most samples or were absent. Fayalite and wüstite, practically mandatory in iron slags, are not evidenced, except for the Vat sample deriving from the Vătava site (Figure 2). The analcime ($NaAlSi_2O_6 \cdot H_2O$) in the 4264 sample (Călugăreni), as well as the clinoclase ($Cu_3AsO_4(OH)_3$) and dolomite ($CaMg(CO_3)_2$) in the Vat (Vătava) sample, could appear accidentally as they aren't really confirmed by the elemental analysis results.

The Vat sample, while poor in quartz, contains olivines (fayalite) and wüstite which indicate that this slag originated most probably from smithing operations.

The differences of the PXRD evidenced mineral content, in accordance with the PXRF and ICP-MS determined elemental compositions suggest that the iron-workers operant at the three different archaeological sites probably used different technologies. The majority of the finds seems to be a primary smithing slag [26]. The amount of the quartz present (acting as flux) is indicative that, at the site, bloom refining probably took place. Silica sand rich soils were added to the smithing hearth, possibly associated with other fluxes, in order to reduce the melting point of the slag, making it easier to squeeze out [6]. Removal of the slag became easier, also increasing the smithing hearth

temperature; the presence of more considerable quantities of cristobalite in the Brâncoveneşti slags suggests processing (slag formation) temperatures from 900 °C to 1200 °C [27].

The iron oxides are indicators of the redox conditions at the time of the slag solidification. The appreciable amount of goethite, a typical weathering mineral formed by wüstite oxidation during burial, indicates mildly reducing conditions. Presumably initially wüstite was the most frequent oxide phase, with minor amounts of magnetite (partially transformed into haematite) [28,29].

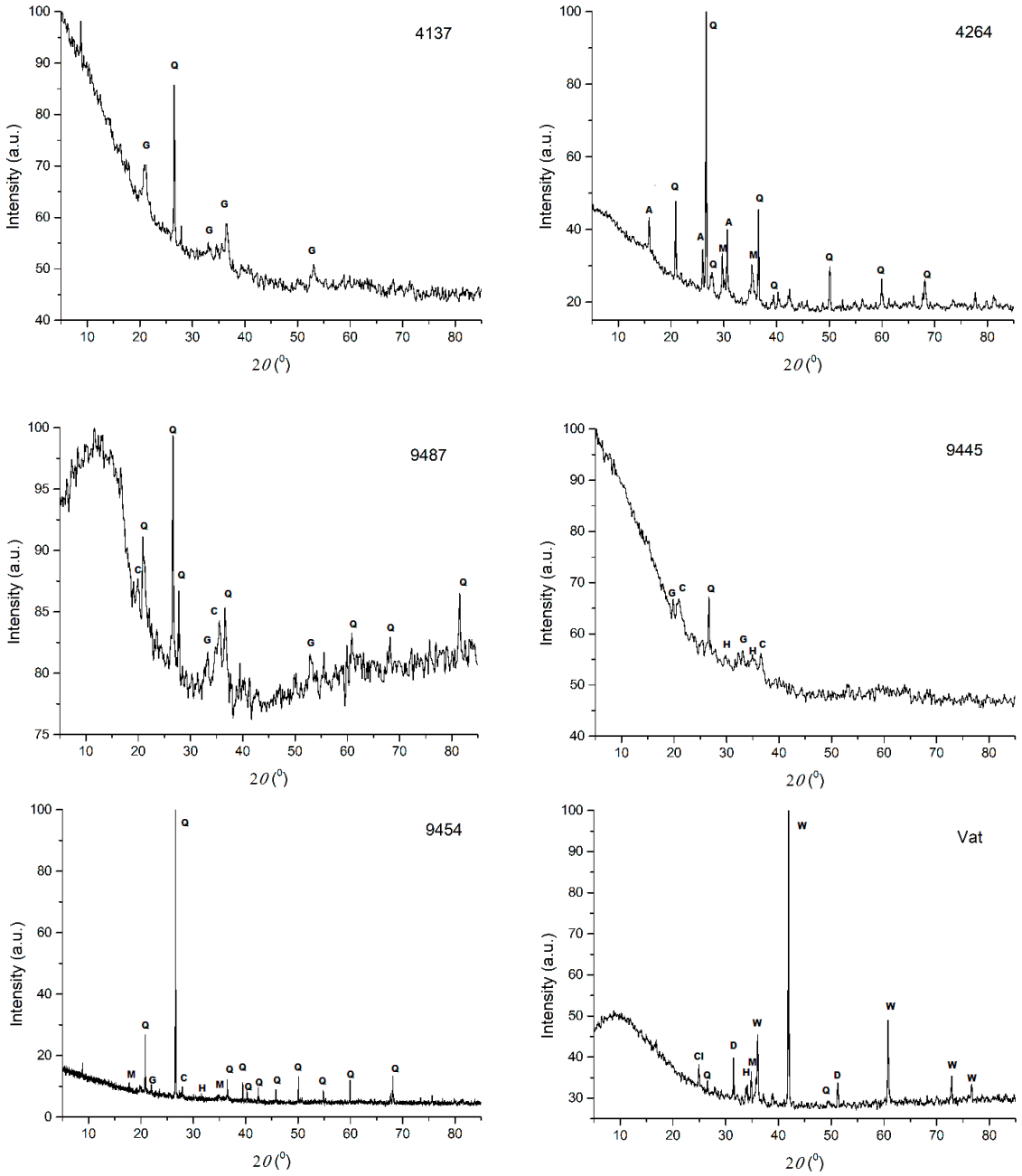

Figure 2. X-ray diffractograms of selected samples. Samples 4137, 4264 are from the Călugăreni (*vicus*) site; 9487, 9445, and 9454 from Brâncoveneşti, the *retentura*; sample Vat is from Vătava, *East of the tower* location. The mineral components notation: Q—quartz; G—goethite; A—analcime; M—magnetite; C—cristobalite; H—hedenbergite; Cl—clinoclase; D—dolomite, W—wüstite.

Table 6. The most abundant PXRD—identified mineral phases of the selected slags.

Mineral Phases	Iron Slag Sample					
	4137	**4264**	**9487**	**9445**	**9454**	**Vat**
	C1/2034	**C1/2038**	**A/1**	**A/3**	**A/3**	**V1**
Quartz	++++	++++	++++	++++	++++	+
Cristobalite	tr	tr	++	++	+	tr
Goethite	+++	tr	++	++	+	tr
Magnetite	tr	+	nd	tr	tr	tr
Hedenbergite	tr	tr	tr	nd	nd	nd
Glassy phase	+++	++	++++	+++	+	+++

++++ majority phase; +++ moderate quantity; ++ small quantity; + very small quantity; tr—traces; nd—not detected.

3.3. FTIR Spectroscopy

FTIR absorption spectra were recorded on both the surface layer and the inside bulk material of the samples in the entire mid-IR region (4000–400 cm^{-1}). However, the mineral composition of the slags could be altered during burial, the alteration process depending on the environmental conditions. The altered layer forms starting from the surface and progresses over time deeper and deeper towards the bulk, the possible modifications affecting primarily the 4000–1500 cm^{-1} (principally OH and CO_2 governed) region of the FTIR spectra. Considering that, for the time being, in this specific case, an adequate study of these aspects is not available, FTIR spectral data interpretation is limited to the less affected 2000–400 cm^{-1} spectral domain (Figure 3).

Except for a few cases (9445 and Vat), the absorption peaks of the FTIR spectra recorded on the outer layer and the inside bulk of the samples in the 2000–400 cm^{-1} domain practically coincide, suggesting that, even if some geochemical processes took place during burial, their influence is mostly negligible. The "deviancy" of some findings probably must be ascribed to specific micro-environmental influences; an adequate explanation would necessitate a deeper investigation of the exact location of the unearthing.

The frequency assignment of the main absorption peaks in the 2000–400 cm^{-1} spectral domain is presented in Table 7; spectral data were interpreted considering literature data published [30–33]. As the FTIR spectra recorded on the outer layer and the inside bulk of the samples in the 2000–400 cm^{-1} region (in most cases) are practically superposed, it can be considered that the FTIR behavior is satisfactorily described by the inside (bulk) data.

With minor differences, Table 7 data indicate a close spectral behavior of the samples, independently from the exact location of their uncovering.

According to the absorption peaks appearing in the spectral domain 2000–400 cm^{-1}, the samples are mainly constituted from silicates, aluminosilicates, and aluminates. Carbonates, formed most probably in environmentally induced carbonation processes occurring during burial, are also present. Other additional differences can also be attributed to burial conditions. The CO_2 peaks on some spectra appeared probably due to the groundwater or humid soil caused deep carbonation.

All this denotes the relative closeness of the smithery practiced on the different locations where most probably the iron objects were processed starting from pig-iron (bloom) of relatively close provenance, using a similar technology.

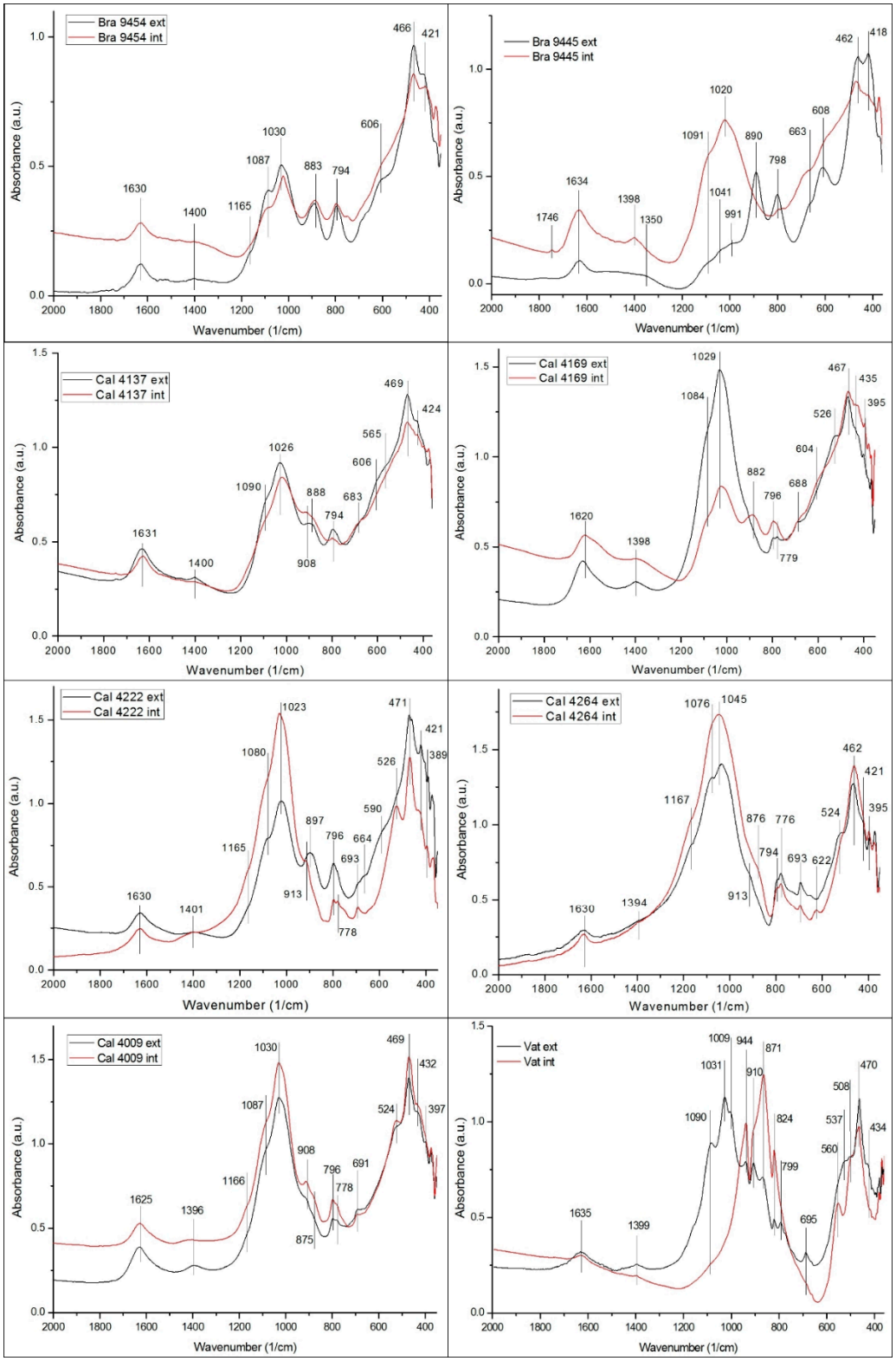

Figure 3. FTIR spectra recorded on the external layer (black line) and on the bulk (red pattern) of the selected samples (Bra: Brâncoveneşti; Cal: Călugăreni; Vat: Vătava).

Table 7. The main FTIR peaks assignment of selected slag sample (bulky matter).

Absorption Frequencies (cm^{-1})										Assignments
4137	**4251**	**4264**	**4009**	**4169**	**4222**	**9487**	**9445**	**9454**	**Vat**	
C1/2034	**C2/2039**	**C1/2038**	**C2/2039**	**C2/2039**	**C1/2038**	**A/1**	**A/3**	**A/3**	**V**	
1631	1627	1630	1625	1620	1630	1631	1634	1630	1635	FeO(OH) 1620–1635
1400	1394	1394 sh	1396	1398	1401	1394		1400 w	1399 sh	CO_3 1390–1410
		1167 sh	1166 sh		1165 sh	1167 sh		1165 sh		SiO_2 1165–1170
1090 sh	1094 sh	1076 sh	1087 sh	1084 sh	1080 sh	1087 sh	1091 sh	1087		SiO_2 1076–1095 FeO(OH) 1105, 1084 Fe_2O_3 1100
1026	1025	1045	1030	1029	1023	1032	1041 sh	1030		SiO_2 1020–1050
						1007 sh	991 sh		944 s	SiO_2 1010–940
908	906 sh	913	908		913 sh	913			910 sh	SiO_2 910–915
		876	875	882			890	883	871 sh	CO_3 890–870
									824 m	FeO(OH) 824
794	789	794	796	796	796	796	798	794		SiO_2 798–789
		776	778	779	778	778				SiO_2 780–775
606 sh							608	606 sh		Fe_2O_3 606–608
565 sh						563 sh			560	FeO(OH) 560–565
	524 sh	524	524	526	526 sh	519				Fe_2O_3 520–526
									508 sh	Fe_3O_4 508
469	467		469	467	471	469	467	466	470	SiO_2 466–470
		462	462 sh							SiO_2 462
	428			435						SiO_2 428–435
424 sh		421			421		418	421		SiO_2 418–424

3.4. EPR Investigation

Smithing slags, very common on archaeological sites, can be classified in three main types, each related to a kind of metallurgical activity [34]. The first type, dominated by fayalite, with a variable amount of iron oxide (mainly wüstite) and a small amount of interstitial glass, is mainly produced by hot oxidation of the metal with a small input of silica from various sources (hearth lining, charcoal, dust, flux) during forging. The second type, richer in silica and minerals deriving from granitic rocks (granites, sandstones, clays) and with low iron content, is produced during fashioning of iron pieces and processing of steel objects. The third type of slag is richer in iron (as metal, oxide, or oxy-hydroxide) contains fayalite and inclusions of charcoal, and is produced during the work of a poorly compacted metal, or when the smith is working close to the melting point of the metal, for example during welding.

Smithing slags are generally formed under reducing conditions controlled by the CO/CO_2 ratio defined by the fluctuating oxygen pressure in the hearth atmosphere. Since formation of the ancient slags is very sensitive to the oxygen content, at the same chemical composition of the melt, it is possible the crystallization of mineral phases with differing Fe^{2+}/Fe^{3+} ratios. This issue can be described with the quartz, fayalite and magnetite (QFM) buffer equilibrium:

$$3\ Fe^{2+}{}_2SiO_4 + O_2 \leftrightarrow 2\ Fe^{2+}Fe^{3+}{}_2O_4 + 3\ SiO_2$$

If the oxygen concentration in the gas atmosphere is sufficiently high, magnetite and a silica-rich compound (like pyroxene) crystallize first. If oxygen is low, no magnetite will be formed, but fayalite (or even metallic iron) precipitates [20].

The Fe^{3+}/Fe^{2+} ratio essentially will be then defined by the raw materials used and the manufacturing technology (the redox conditions which occur during the metallurgical process of iron processing). The knowledge of the Fe^{3+}/Fe^{2+} ratio could enable the samples' identification as primary (bloom refining) or secondary (iron bar processing) smithing slags [26].

EPR spectroscopy is widely used in materials research, predominantly in structural investigations [35,36], and also has applications in geological and archaeological dating [37]. As the quantitative analytical method performs only occasionally, mostly in studies carried out on Fe and Mn containing clays, glasses, and ceramics. As the reliable standardization assuring the avoidance of matrix related errors in this case is difficult, EPR spectroscopy only delivers semiquantitative results [38]. However, semiquantitative data permit the adequate determination of the Fe^{3+}/Fe^{2+} ratio; in addition, the method has the advantage of simple and easy sample preparation, without the need for expensive standards, costly, and/or hazardous chemicals.

Experimental EPR spectra recorded for Fe_2O_3 at room temperature (a broader line superposed on a narrow line) are typical superparamagnetic resonance spectra. The broad component of the EPR signal shifts left with increasing Fe_2O_3 concentration; the narrow one is observed at the same field~3500 G ($g = 2$) regardless of concentration. With the increase in the Fe_2O_3 concentration, the narrow component also broadens and becomes less visible until it is completely unobservable in the highly concentrated samples [35–40].

The integrated intensity I of the EPR signal (area beneath the absorption curve) is proportional to the concentration of the paramagnetic centers in the sample. EPR spectral features (I) recorded at room temperature on the untreated sample specimens (e.g., before any thermal treatment) correspond to the presence of the Fe^{3+} paramagnetic centers alone, since, above 77 K, the resonance assigned to Fe^{2+} can't be detected. $I_{Fe(tot)}$ can be obtained from the room temperature spectrum of the same specimen after the quantitative oxidation of the Fe^{2+} content to Fe^{3+}. This may be achieved keeping the finely pulverized slag at 300 °C in the presence of air atmospheric for 6 h proved to assure the quantitative oxidation of Fe^{2+} to Fe^{3+}. The ferrous iron quantity will be the difference of the integrated intensities ($I_{Fe(tot)}$–$I_{Fe(III)}$).

The experimental EPR spectra recorded on selected samples are presented in Figure 4.

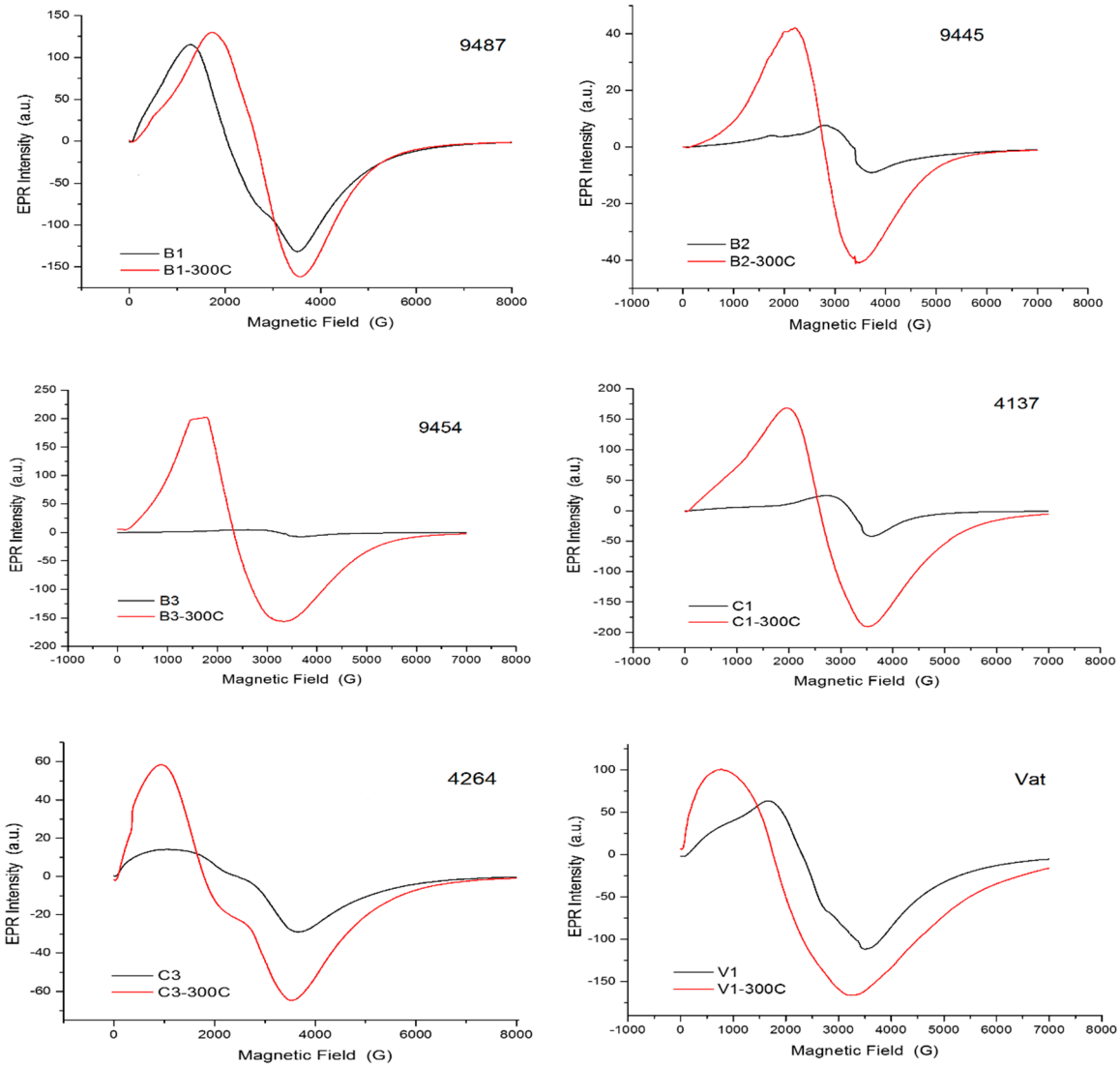

Figure 4. EPR spectra of selected samples: 9487 (B1), 9445 (B2), 9454 (B3) from Brâncoveneşti; 4137 (C1), 4264 (C3) from Călugăreni; and Vat (V1) from Vătava. Black spectra were recorded on the untreated samples; red spectra after thermal treatment applied.

Table 8 contains the calculated Fe^{3+}/Fe^{2+} ratio values from experimental results.

Table 8. Experimental Fe^{3+}/Fe^{2+} ratio of the investigated samples.

Sample	$10^8 \cdot I_{Fe(III)}$	$10^8 \cdot I_{Fe(tot)}$	$10^8 \cdot I_{Fe(II)}$	Fe^{3+}/Fe^{2+}
9487	3.30	4.13	0.83	3.976
9445	0.23	1.05	0.82	0.280
9454	0.13	4.92	4.79	0.027
4137	0.61	5.60	4.98	0.122
4264	0.75	1.79	1.04	0.721
Vat	2.52	3.88	1.36	1.853

$I_{Fe(III)}$, $I_{Fe(tot)}$, $I_{Fe(II)}$ are the correspondent integrated intensities.

As shown by the experimental spectra presented in Figure 4 and the data from Table 8, the EPR method can be used to characterize the redox conditions of slag formation even if, due to the pronounced

heterogeneity of the samples, the (obviously only local) data obtained in this way can't be extended to the whole of the sample. The Fe^{3+}/Fe^{2+} ratio values of Table 8 are calculated from EPR measurements realized on probes of amounts of only few milligrams. The "unreliability of global conclusions" results also when the data from Table 8 are compared to those from Table 6.

Still, the differences of the Fe^{3+}/Fe^{2+} resulting ratios are able to suggest successfully the differing redox ambience during the slag formation caused by the supposedly different working conditions. All finds can be considered smithing slags; however, the iron-workers operant at the three different archaeological sites should use different technologies. The considerable amount of quartz present in the Brâncoveneşti and Călugăreni samples suggests second type smithing slags, the quartz deriving from silica sand rich soils added to the smithing hearth as flux, while the findings from Vătava seem to be third type smithing slags [34].

The iron oxides could be indicators of the redox conditions at the time of the slag solidification. The appreciable amount of goethite, a typical weathering mineral, indicates mildly reducing conditions.

4. Conclusions

Surface screening of the slag samples with a hand-held XRF spectrometer confirms that, compositionally, they are highly heterogeneous. Elemental compositions suggest the different provenance of the raw materials.

Chemical composition as well as structural analyses permit affirming that at least bloom refining and processing of the refined iron took place on the sites. The slag cakes found could be byproducts of the refining process carried out in pit-furnaces [34]. The Fe dominancy in all the samples (even in the Vat sample which is the poorest in iron) can be attributed to the presence of a significant quantity of metallic globules (probably alloyed iron) embedded in the slags and formed during primary and/or secondary smithing.

Mineralogically, archaeological iron slags are a heterogeneous mixture of silicates (olivines like fayalite, pyroxenes like hedenbergite), iron oxides (wüstite, magnetite), amorphous material (mostly glass phases), and alteration products (like goethite). The FTIR spectral data indicate the presence of mineral phases expected in different (primary and/or secondary) smithing slag types. Corresponding to the PXRD data, in accordance with the FTIR results, besides the generally dominant quartz and a relatively great amount of amorphous, mostly glassy material, the main mineral phases of the Brâncoveneşti and Călugăreni samples are the pyroxene hedenbergite, the iron oxyhydroxide goethite and the iron oxide magnetite—while, in the case of the Vătava sample, the same iron oxides and (not seen by XRD) the olivine fayalite.

PXRD and FTIR results suggest that the studied slags can be considered primary or secondary smithing debris (metallurgical waste produced in the last steps of the smithing operations carried out by the blacksmith). Primary smithing slags are generated during the refining of the bloom, and secondary smithing slags are formed during the manufacturing and/or repair of artifacts [26].

The PXRD identified minerals are formed as the result of a complex smithing process supposing different temperature regimes. Hedenbergite, the predominant pyroxene of the slags from Brâncoveneşti and Călugăreni, is segregated at crystallization temperatures ranging from 700 to 900 °C; olivines (the fayalite appearing on the diffractogram recorded on the Vătava sample—see Figure 2) crystallize at 1100–1200 °C; the presence of cristobalite also indicates the achievement of high temperatures during the metal processing. The quartz found in all samples derives most probably from flux addition. The most frequent iron oxide phase, associated with minor amounts of magnetite, is wüstite, practically degraded during burial. The omnipresent weathering mineral goethite is formed in the course of wüstite oxidation [31,34].

The EPR spectra are able to properly prove the presence of Fe^{3+} ions in the samples, the method allowing the determination of the Fe^{3+}/Fe^{2+} ratio in fair agreement with the chemical analysis data and the mildly reducing conditions of the slag solidification indicated by the amount of goethite (formed mostly by wüstite oxidation during burial) typically present in the samples.

Author Contributions: Conceptualization, E.B. and S.-P.P.; methodology, E.B., S.-P.P., and E.V.; investigation, data curation I.K., C.T., G.B., D.T. and Z.K.-B.; resources, E.B.; writing—original draft preparation, E.V., I.K., C.T., G.B., and Z.K.-B.; writing—review and editing, E.B. and S.-P.P. All authors have read and agreed to the published version of the manuscript.

Funding: The PXRD: FTIR and EPR measurements were financially supported by the Romanian Ministry of Research and Innovation, Core Program, Projects PN 19 35 02 01 and PN19 35 02 03.

Acknowledgments: The archaeometric (archaeometallurgical) research carried out is part of the Project for Technical and Cultural Heritage Preservation in Transylvania, initiated and supervised by the Research Institute of the Transylvanian Museum Society. The financial support was assured by the 2018–2019/HTMT grant of the Homeland Research Program supervised by the Hungarian Science Abroad Presidential Committee of the Hungarian Scientific Academy. From 2013, the field research from Călugăreni was organized as archaeological field school, involving the participation of students and lecturers of archaeology, geophysics, architecture, conservation, and restoration from the University of Cologne, the University of Pécs, the Budapest University of Technology and Economics, the Eötvös Loránd University, the University of Applied Sciences Erfurt, the Babeş–Bolyai University of Cluj-Napoca, and the Petru Maior University of Târgu Mureş, as part of the international interdisciplinary project *The Roman Limes as a European Cultural Landscape* coordinated by the Mureş County Museum and the Winckelman Institute of the Humboldt University of Berlin. Since 2016, the research was financed by the Mureş County Council, the Chair of the Roman Provinces at the Archaeological Institute of the University of Cologne, the Erasmus Fund of the Humboldt University of Berlin, and the Romanian Ministry of Culture. The excavation from Brâncovenești and Vătava have been organized by the Mureş County Museum and financed by the Mureş County Council.

Conflicts of Interest: The authors declare no conflict of interest.

References

1. Pánczél, S.P.; Lenkey, L.; Pethe, M.; Laczkó, N. Updating our Knowledge about the Roman Fort from Brâncovenești, Mureș County. *Marisia* **2012**, *32*, 105–115.
2. Pánczél, S.P.; Mustaţă, S.; Dobos, A. The Research at the Roman Auxiliary Fort of Mikháza/Călugăreni. *Magy. Régészet/Hung. Archaeology* **2018**, *2018/1*, 13–20.
3. Dobos, A.; Fiedler, M.; Höpken, C.; Mustaţă, S.; Pánczél, S.P. Militärlager und vicus in Călugăreni/Mikháza (Kreis Mureş, Rumänien) am Dakischen Ostlimes. *KuBA* **2017**, *7*, 145–154.
4. Szabó, M.; Pánczél, S.P.; Cioată, M.D. Római kori lelőhelyek kutatása a Kelemen-havasok lábánál. In *Várak, Kastélyok, Templomok Évkönyv*; Kósa, P., Ed.; Zöld Infó Média: Pécs, Hungary, 2017; pp. 116–119.
5. Ingoglia, C.; Triscari, M.; Sabatino, G. Archaeometallurgy in Messina: Iron slag from a dig at block P, laboratory analyses and interpretation. *MAA* **2008**, *8*, 49–60.
6. Scott, R.B.; Eekelers, K.; Degryse, P. Quantitative chemical analysis of archaeological slag material using handheld X-ray fluorescence spectrometry. *Appl. Spectrosc.* **2016**, *70*, 94–109. [CrossRef] [PubMed]
7. Nemet, I.; Rončević, S.; Bugar, A.; Ferri, T.Z.; Pitarević, L. Classification analysis of archaeological findings from early-iron production (Turopolje region, NW Croatia) based on multi-analytical profiling. *JAAS* **2018**, *33*, 2053–2061. [CrossRef]
8. Bitay, E.; Kacsó, I.; Pánczél, S.P.; Veress, E. Comparative Study of Roman Iron Slags Discovered in the Roman Auxiliary Fort and Settlement of Călugăreni. *Acta Mat. Transyl.* **2018**, *1*, 65–72. [CrossRef]
9. Lemiere, B. A review of pXRF (field portable X-ray fluorescence) applications for applied geochemistry. *J. Geochem. Explor.* **2018**, *188*, 350–363. [CrossRef]
10. Hunt, A.M.; Speakman, R.J. Portable XRF analysis of archaeological sediments and ceramics. *J.Archaeol. Sci.* **2015**, *53*, 626–638. [CrossRef]
11. Bačeva, K.; Stafilov, T.; Šajn, R.; Tănăselia, C.; Makreski, P. Distribution of chemical elements in soils and stream sediments in the area of abandoned Sb–As–Tl Allchar mine, Republic of Macedonia. *Environ. Res.* **2014**, *133*, 77–89. [CrossRef]
12. Levei, E.; Frenţiu, T.; Ponta, M.; Tănăselia, C.; Borodi, G. Characterization and assessment of potential environmental risk of tailings stored in seven impoundments in the Aries river basin, Western Romania. *Chem. Cent. J.* **2013**, *7*, 14. [CrossRef] [PubMed]
13. Bitay, E.; Kacsó, I.; Toloman, D.; Pánczél, S.P.; Veress, E. EPR spectroscopic determination of the Fe(II)/Fe(III) ratio in roman slags from Brâncovenești (Marosvécs), Călugăreni (Mikháza) and Vătava (Felsőrépa), Romania. *Papers Tech. Sci.* **2017**, *7*, 103–106.

14. Misra, M.K.; Ragland, K.W.; Baker, A.J. Wood ash composition as a function of furnace temperature. *Biomass Bioenerg.* **1993**, *4*, 103–116. [CrossRef]
15. Chowdhury, S.; Mishra, M.; Suganya, O.M. The incorporation of wood waste ash as a partial cement replacement material for making structural grade concrete: An overview. *Ain Shams Eng. J.* **2015**, *6*, 429–437. [CrossRef]
16. Griffith, D.A.; Johnson, D.L.; Hunt, A. The geographic distribution of metals in urban soils: The case of Syracuse, NY. *GeoJournal* **2009**, *74*, 275–291. [CrossRef]
17. Al Maliki, A.; Al-lami, A.K.; Hussain, H.M.; Al-Ansari, N. Comparison between inductively coupled plasma and X-ray fluorescence performance for Pb analysis in environmental soil samples. *Environ. Earth Sci.* **2017**, *76*, 433. [CrossRef]
18. Molnár, F. Salakok és fémek archeometriai vizsgálata. In *Régészeti kézikönyv*; Müller, R., Ed.; Magyar Régész Szövetség: Budapest, Hunagary, 2011; pp. 510–524.
19. Charlton, M.F.; Blakelock, E.; Martinón-Torres, M.; Young, T. Investigating the production provenance of iron artifacts with multivariate methods. *J. Archaeol. Sci.* **2012**, *39*, 2280–2293. [CrossRef]
20. Hauptmann, A. The investigation of archaeometallurgical slag. In *Archaeometallurgy in Global Perspective. Methods and Syntheses*; Roberts, B.W., Thornton, C.P., Eds.; Springer: New York, NY, USA, 2014; pp. 91–105.
21. Andersson, D. Iron-working at Hornlandsudde: Archaeometallurgic analyses: Rogsta Parish, Hälsingland. In *GAL Analysrapport 7-2007*; Riksantikvarieämbetet, Avdelningen för arkeologiska undersökningar: Stockholm, Sweden, 2007; 12p.
22. Kramar, S.; Lux, J.; Pristacz, H.; Mirtic, B.; Rogan-Smuc, N. Mineralogical and geochemical characterization of Roman slag from the archaeological site near Mosnje (Slovenia). *Mater. Technol. (MTAEC9)* **2015**, *49*, 343–348. [CrossRef]
23. Mateus, A.; Pinto, A.; Alves, L.C.; Matos, J.X.; Figueiras, J.; Neng, N.R. Roman and modern slag at S. Domingos mine (IPB, Portugal): Compositional features and implications for their long-term stability and potential reuse. *IJEWM* **2011**, *8*, 133–159. [CrossRef]
24. Sheikh, M.R.; Acharya, B.S.; Gartia, R.K. Characterization of iron slag of Kakching, Manipur by X-ray and optical spectroscopy. *IJPAP* **2010**, *48*, 632–634.
25. Mohassab, Y.; Sohn, H.Y. Application of spectroscopic analysis techniques to the determination of slag structures and properties: Effect of water vapor on slag chemistry relevant to a novel flash ironmaking technology. *JOM* **2013**, *65*, 1559–1565. [CrossRef]
26. McDonnell, J.G. A model for the formation of smithing slags. *Mater. Archeol.* **1991**, *26*, 23–26.
27. Gotić, M.; Musić, S. Mössbauer, FT-IR and FE SEM investigation of iron oxides precipitated from $FeSO_4$ solutions. *J. Mol. Struct.* **2007**, *834–836*, 445–453. [CrossRef]
28. Kramar, S.; Lux, J.; Mladenović, A.; Pristacz, H.; Mirtič, B.; Sagadin, M.; Rogan-Šmuc, N. Mineralogical and geochemical characteristics of Roman pottery from an archaeological site near Mošnje (Slovenia). *Appl. Clay Sci.* **2012**, *57*, 39–48. [CrossRef]
29. Di Bella, M.; Aleo Nero, C.; Chiovaro, M.; Italiano, F.; Quartieri, S.; Romano, D.; Leonetti, F.; Marcianò, G.; Sabatino, G. Archaeometric study of the hellenistic metallurgy in Sicily: Mineralogical and chemical characterization of iron slags from punic Panormos (Palermo, Italy). *MAA* **2018**, *18*, 127–139.
30. Merzbacher, C.I.; White, W.B. The structure of alkaline earth aluminosilicate glasses as determined by vibrational spectroscopy. *J. Non-Cryst. Solids* **1991**, *130*, 18–34. [CrossRef]
31. ElBatal, H.A.; Ghoneim, N.A.; Ouis, M.A. Preparation and characterization of glass and glass-ceramics from industrial waste materials including iron slag and cement dust. In Proceedings of the ICCM-17–17th International Conference on Composite Materials, Edinburgh, UK, 27–31 July 2009; Available online: http://www.iccm-central.org/Proceedings/ICCM17proceedings/Themes/Industry/ADV%20COMP%20MATS%20IN%20CONSTRUCTION/INT%20-%20ADV%20COMP%20MATS%20IN%20CONSTR/IA1.2%20Ouis.pdf (accessed on 20 June 2020).
32. Olovčić, A.; Memić, M.; Žero, S.; Huremović, J.; Kahrović, E. Chemical analysis of iron slags and metallic artefacts from early iron age. *Int. Res. J. Pure Appl. Chem.* **2014**, *4*, 859–870. [CrossRef]
33. Kloprogge, J.T.; Wharton, D.; Hickey, L.; Frost, R.L. Infrared and Raman study of interlayer anions CO_3^{2-}, NO_3^-, SO_4^{2-} and ClO_4^- in Mg/Al-hydrotalcite. *Am. Mineral.* **2002**, *87*, 623–629. [CrossRef]

34. Serneels, V.; Perret, S. Quantification of smithing activities based on the investigation of slag and other material remains. In Proceedings of the International Conference Archaeometallurgy in Europe, Milano, Italy, 24–26 September 2003; Associazione Italiana di Metallurgia: Milano, Italy, 2003; Volume 1, pp. 469–478.
35. Prakash, C.; Husain, S.; Singh, R.J.; Mollah, S. Electron paramagnetic resonance of Fe^{3+} ions in Bi_2O_3–PbO–Fe_2O_3 glasses. *J. Alloy. Compd.* **2001**, *326*, 47–49. [CrossRef]
36. Roessler, M.M.; Salvadori, E. Principles and applications of EPR spectroscopy in the chemical sciences. *Chem. Soc. Rev.* **2018**, *47*, 2534–2553. [CrossRef]
37. Bhattacharyya, A.; Schmidt, M.P.; Stavitski, E.; Martínez, C.E. Iron speciation in peats: Chemical and spectroscopic evidence for the co-occurrence of ferric and ferrous iron in organic complexes and mineral precipitates. *Org. Geochem.* **2018**, *115*, 124–137. [CrossRef]
38. Hofmeister, A.M.; Rossman, G.R. Determination of Fe^{3+} and Fe^{2+} concentrations in feldspar by optical absorption and EPR spectroscopy. *Phys. Chem. Miner.* **1984**, *11*, 213–224. [CrossRef]
39. Koksharov, Y.A.; Pankratov, D.A.; Gubin, S.P.; Kosobudsky, I.D.; Beltran, M.; Khodorkovsky, Y.; Tishin, A.M. Electron paramagnetic resonance of ferrite nanoparticles. *J. Appl. Phys.* **2001**, *89*, 2293–2298. [CrossRef]
40. Noginov, M.M.; Noginova, N.; Amponsah, O.; Bah, R.; Rakhimov, R.; Atsarkin, V.A. Magnetic resonance in iron oxide nanoparticles: Quantum features and effect of size. *J. Magn. Magn. Mater.* **2008**, *320*, 2228–2232. [CrossRef]